Adsorptive Recovery of Crude Oil Microdroplets from Wastewater Using Surface Engineered Sponges

Pavani Cherukupally, Wei Sun, Anabelle P.Y. Wong, Daryl R. Williams, Geoffrey A. Ozin, [*] Amy M. Bilton, [*] and Chul B. Park[*]

Abstract

In the US, the oil industry produces over 15 billion barrels of wastewater contaminated with crude oil microdroplets annually. Current technologies are unable to remove these microdroplets at different pH conditions. Herein, an innovative surface engineered sponge (SEnS) was designed by combining surface chemistry, surface charge, roughness, and surface energy. Under all pH conditions, the SEnS rapidly adsorbed oil microdroplets with 95-99% removal efficiency predominantly by Lifshitz-van der Waals forces. Furthermore, at the best pH value, 92% of the oil was adsorbed within 10 min due to synergistic Lifshitz-van der Waals and acid-base (electrostatic attractive interactions and hydrogen bond) forces. The adsorbed crude oil was recovered at ambient conditions while the cleaned SEnS was reused up to five times for crude oil adsorption. Due to the process efficacy, sponge reuse, and oil recovery, this adsorptive-recovery method using SEnS demonstrates great potential for the industrial recovery of oil from wastewater.

Introduction

In the US, the oil industry produces over 15 billion barrels of wastewater annually.[1] Oil extraction, processing, and accidental spills frequently generate crude oil microdroplets (<20 μm). These difficult-to-remove microdroplets have adverse effect on the ecosystem.[2,3] Cost-effective methods for microdroplet recovery, especially at pH conditions commonly seen in oil field wastewater, do not currently exist and are essential to minimize environmental impacts. Among physical separation methods, adsorption is desirable due to its low cost, energy-efficiency, and wide applicability.[4] However, traditional nanoporous adsorbents, such as activated carbon, are incompatible with micrometer-sized droplets.[4-6]

Recently, surface engineered sponges (SEnS) have emerged as promising adsorbents for oil microdroplets.[7-9] Due to their low cost, ease of fabrication, and high uptake capacity, sponges have great potential as industrial-scale sorbents.[10] To date, most sponge surfaces have been tailored to adsorb surfactant-stabilized pure hydrocarbon emulsions, which exhibit monotonous wetting at different pH values.[7,8] In contrast, crude oil is a complex mixture of ionic, polar, and non-polar components.[11,12] As a result, depending on pH, these complex chemical mixtures can exhibit large variability in physicochemical properties[13,14] leading to a broad range of contact angles at a solid surface.[9] Furthermore, the fundamental mechanisms governing variation in crude oil wetting behaviour with pH, which are important for material design, are not well understood.

This work develops new sponges that are robust to the variable pH-responsive wetting behaviour of crude oil. Desirable sponge surface properties for microdroplets adsorption over broad pH conditions were hypothesized. To complement crude oil composition variability, the sponge surface is predicted to need organic, acid and base sites for effective oil adsorption (**Figure 1a**). Along with tailored surface chemistry,[15-17] the surface charge,[17-19] and roughness[20-22] may also invoke favorable wetting behavior[23-26] at the sponge surface (**Figure 1b**), enabling adsorption of oil droplets over a broad pH range. Based on these properties, the crude oil adsorption process efficacy can be predicted and validated experimentally.

Herein, the aforementioned approach was applied to develop SEnS for adsorptive recovery of crude oil microdroplets for variable pH conditions. The SEnS consists of an acid-base polyester

polyurethane sponge coated with decyl capped nanocrystalline silicon. The surface chemistry, surface charge, roughness, and surface energy were characterized using X-ray photoelectron spectroscopy, microscopy, electrokinetic analysis, and inverse chromatographic techniques. Based on the surface energy and surface charge properties, the microdroplet adsorption efficacy with pH was predicted. Experiments showed the SEnS rapidly physisorbed microdroplets at all pH values with 95-99% efficiency, predominantly by Lifshitz-van der Waals forces. Furthermore, at the best pH value, due to synergistic Lifshitz-van der Waals forces, electrostatic forces, and hydrogen bonding, over 92% of the oil was adsorbed within 10 minutes. Subsequently, the adsorbed crude oil was recovered at ambient conditions by surface displacement using a solvent. The cleaned SEnS was reused five times for microdroplets adsorption. This new framework opens pathways for development of innovative SEnS and the evolution of sponge-based adsorption technologies to remediate oil field effluents.
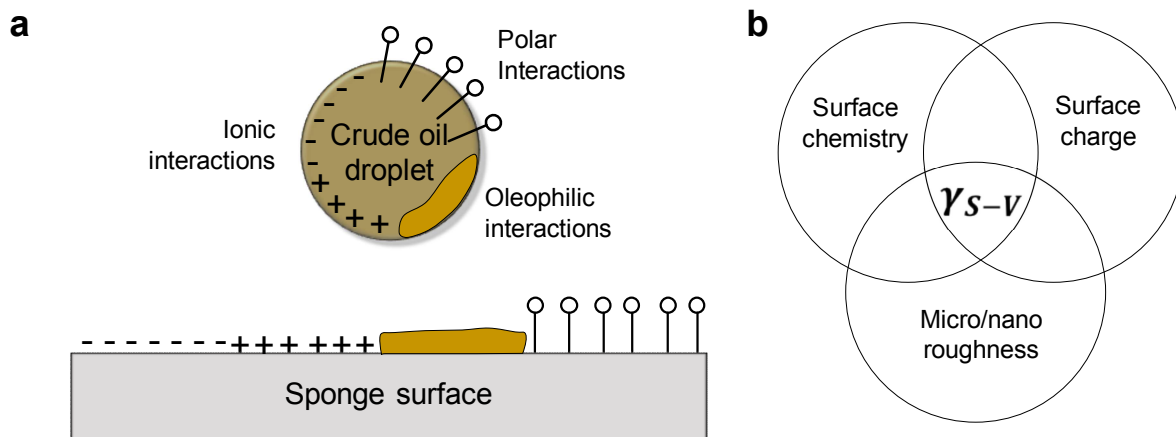
Figure 1. Approach followed in this work: (a) Problem statement - to compensate for variations in crude oil composition, the rational design of the sponge surface chemistry includes acid, base, and hydrophobic/oleophilic groups. These heterogeneous chemical groups evoke attractive interactions between the sponge and crude oil microdroplets to enable effective wetting and adhesion to the sponge surface through adsorptive capture. (b) Our solution - primary surface characteristics manipulated to achieve the desired surface energy (γ_{S-V}) for effective wetting and adhesion of the crude oil microdroplets at different pH conditions.

Results & Discussion

Material selection and characterization. In this work, PESPU sponge with pore size of 200-1100 μm and porosity of ~97% was used as a 3D substrate due to its complementary acid-base surface groups and high porosity.[9] Facile dip-coating was selected as the technique to functionalize the sponge surface with organic groups, to incorporate nanoroughness, and to manipulate the surface energy. Among currently available nanomaterials for coating the sponge, silica-based nanomaterials are favorable due to their earth abundancy and nontoxicity. Therefore, in this work, green nanocrystalline silicon (ncSi) was selected to enable future application in photochemical degradation of hydrocarbons in wastewater.

Recently, research has shown that nanomaterials with spherical asperity shape and size of ~100 nm are advantageous due to their abrasion resistance,[27] slow degradation,[28] and higher amount of adsorbate attachment.[29] Our experiments also showed that both 20 nm and 100 nm ncSi:C10 exhibit approximately equal rates of crude oil removal (**Figure S1**). Since, the commercial 100 nm ncSi was more cost-effective, this particle size was used to functionalize the sponge. Therefore, functionalized decyl with ncSi at <1 wt% was used to coat the PESPU sponge. The resulting composite, referred to as a SEnS, possessed a surface area of 11.12 $m^2 g^{-1}$.

Surface chemistry. The presence of acid, base and hydrophobic/oleophilic groups on the SEnS surface was verified using X-ray photoelectron spectroscopy (XPS) and inverse gas chromatography (IGC). The XPS survey spectrum reveals the presence of C, O, N, Cl, and Si (**Figure 2a**). The measured elemental composition ratios of C/O and C/N were 6.18 and 18.85, respectively indicating high concentrations of carbon. This is directly related to desirable oleophilic sites. In C 1s spectrum (**Figure 2b**), the peaks at 285.0, 286.6, and 289.3 eV are attributed to C-C or C-H, NH-COO, and COOH, respectively. These features are consistent with the structures of polyester and polyurethane which contribute to acid and base sites. The strong C-C peak relative to other peaks is attributed to the ncSi:C10 deposition. The low intensity of the COOH is ascribed to the loose carboxylic groups from esters.[30] The high-resolution N 1s spectrum of the sample shows two peaks (**Figure 2c**). The stronger peak of the nitrogen is assigned to primary amino groups (399.8 eV), the weaker peak is in the form of protonated or hydrogen-bonded amine (401 eV).[31] In the Si 2p spectrum (**Figure 2d**), the peak at 100 eV is ascribed to Si (0) of the ncSi core, while the peak at 102.5 eV region is ascribed to Si-C and Si surface sub-oxides on the ncSi surface.[32] The ncSi contributes to hydrophobic sites at the sponge surface.

The relative Lewis acid and base composition of the SEnS was determined using IGC according to Gutmann approach (**Figure 2e**).[33,34] Dichloromethane and ethyl acetate were used as the probe molecules to estimate the acid (K_a) and base (K_b) numbers. The measurements showed the K_a number (electron acceptor or proton donor) was 0.14 and the K_b number (electron donor and proton acceptor) was 0.7. Therefore, the SEnS is amphoteric and predominantly Lewis base could be due to lower number of carboxylic and higher number of amine groups.[18,35,36] In conclusion, the XPS and IGC analyses reveal that the SEnS contains acid, base, oleophilic, and hydrophobic sites at the surface. These groups enable adsorption of the crude oil microdroplets by complimentary heterogeneous chemical groups.

Surface charge. The solution pH is another critical factor affecting the material surface charge (ζ potential) and adsorption properties. It provides a measure of the magnitude and sign of the charge associated with the electrical double layer on the sponge surface.[37,38] **Figure 2f** shows the ζ potential of SEnS in 0.001 M KCl solution at different pH conditions. The zeta potential of the SEnS was calculated from streaming potential using the Smoluchowski equation (1):

$$\zeta = \frac{dI}{dp} \cdot \frac{\eta}{\epsilon \epsilon_0} \cdot \frac{L}{A} \tag{1}$$

where, dI/dp is slope of streaming potential versus differential pressure, η is electrolyte viscosity, ϵ is dielectric coefficient of electrolyte, ϵ_0 is permittivity, L is length of the streaming channel, and A is the cross-section of the streaming channel. As can be seen, the point of zero charge (PZC) of the SEnS was found to be at pH 6.3. Below the PZC, the sponge is positively charged and above the PZC, it is negatively charged. The positive charge at lower pH values is ascribed to the preferential adsorption of H_3O^+ ions and negative charge at higher pH values is attributed to the preferential adsorption of the OH^- ions onto the SEnS surface.[39]
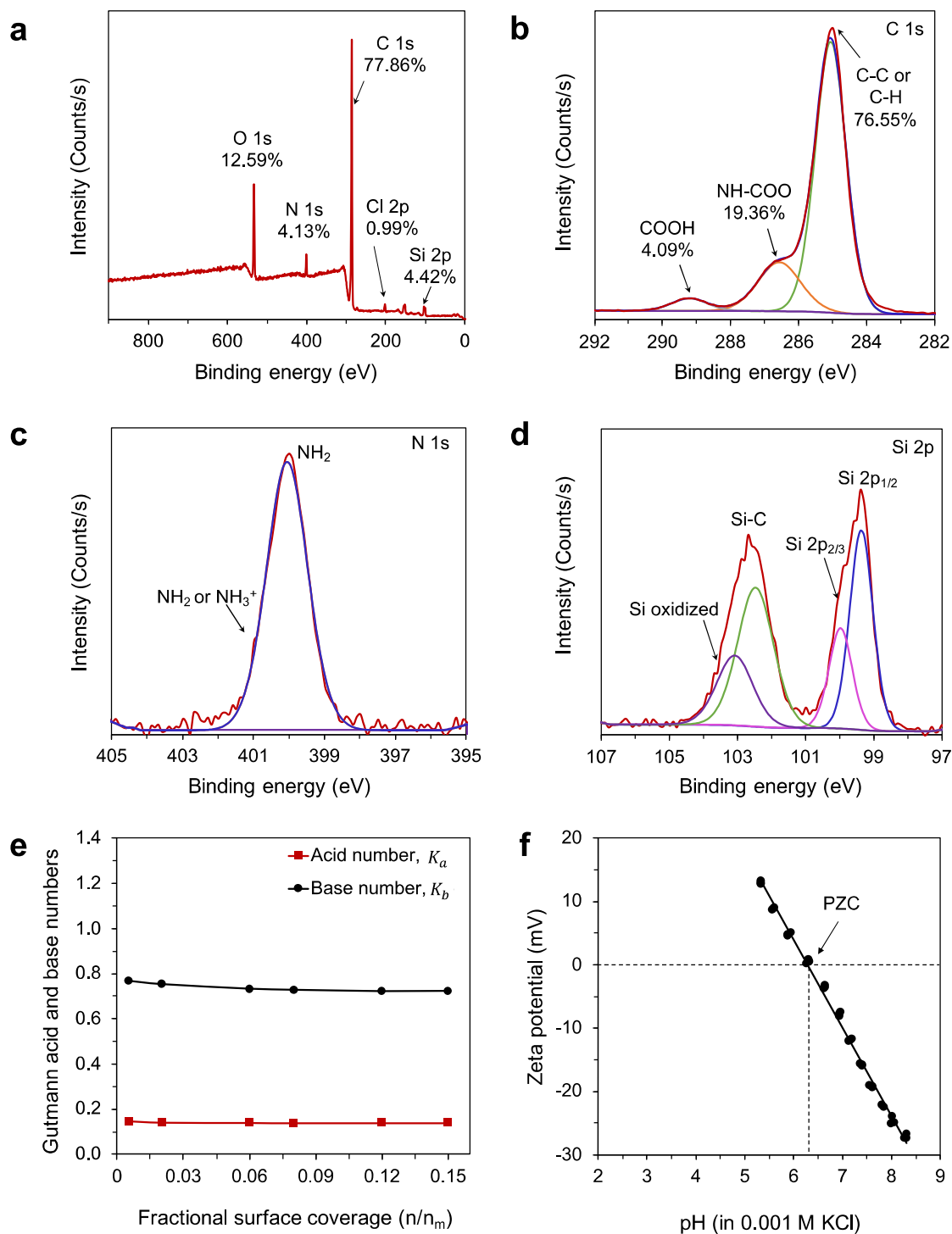
Figure 2. SEnS surface characterization: (a) to (d) Using XPS, (a) survey spectra with elemental atomic percentages, (b) C 1s, (c) N 1s, and (d) Si 2p spectra. (e) Acid and base profiles obtained using IGC. (f) ζ potential versus pH showing the point of zero charge of the SEnS.

Multiscale roughness. The micro/nano roughness plays an important role in wetting properties at solid surfaces. **Figure 3** shows the surface morphological features at the SEnS surface. The field emission scanning electron microscopy (FESEM) images show ncSi:C10 aggregates deposited on the struts of the sponge surface. Due to pre-existing micro crevices on the struts surface, the ncSi:C10 addition forms micro/nano or double roughness profile (**Figure 3a** to **3d**). The nanostructures at the SEnS film surfaces were visualized using atomic force microscopy (**Figure S2**). The nanoroughness was in the range of 60-250 nm and were spiky, reflecting the typical shape of hydrophobic particles.[20] The global surface roughness (R_a value) measured using the optical profiler was approximately 51 μm (**Figure 3e**).

It is well known that the double roughness profile at a solid surface could result in hydrophobicity, corrosive resistance, and self-cleaning properties.[22] The surface wettability of water and crude oil inside the SEnS was observed using *in-situ* micro computed tomography (micro-CT). In **Figure 3f**, the white zones show water draining through the pores which is not adhering to the surface due to the hydrophobic nature of the pores. In contrast, the crude oil, shown as the pink zones in **Figure 3g**, spontaneously wet the pores due to oleophilic decyl groups. **Figure S3** shows the SEnS also exhibits good stability against water, 0.1 M hydrochloric acid, and 0.1 M sodium hydroxide. Therefore, the SEnS could be expected to perform well in a harsh pH environment. The SEnS has also exhibited good self-cleaning properties (**Figure S4**).
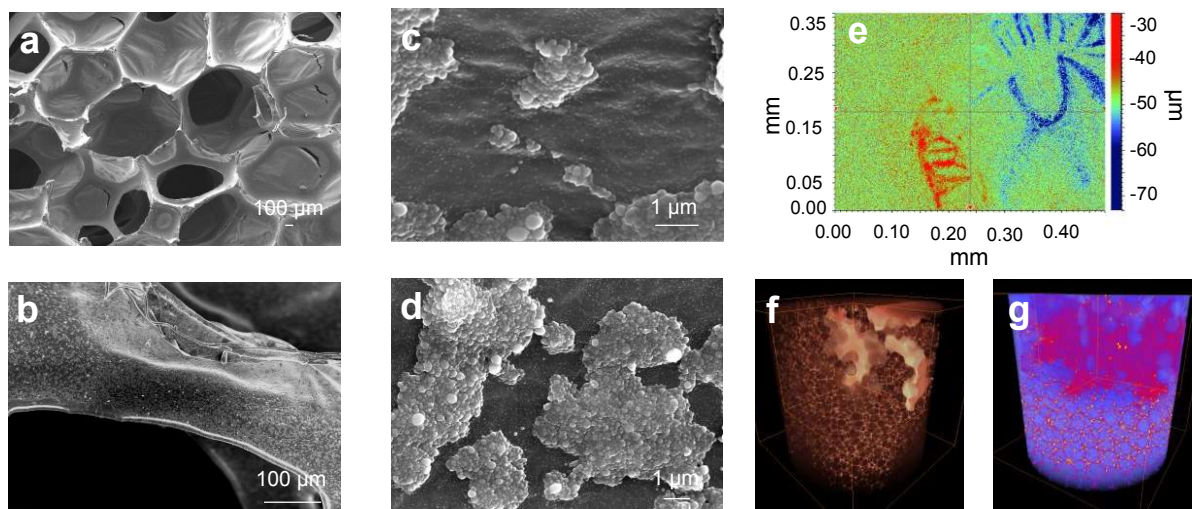
Figure 3. Influence of ncSi:C10 coating on the SEnS surface roughness: (a) to (d) FESEM micrographs at different magnifications. (e) Optical profile of the SEnS showing overall surface roughness. (f) and (g) Visualization of hydrophobic-oleophilic properties of the SEnS using *in-situ* micro-CT. Wetting behavior (f) with water and (g) with crude oil.

Critical surface energy. The SEnS surface physicochemical features were modified using ncSi:C10 to achieve critical or total surface energy to maximize crude oil micro droplet wetting and adsorption. The IGC technique was used to measure the total (γ_{S-V}), dispersion (γ_{LW}), and acid-base (γ_{AB}) contributions to the surface energies of the SEnS. Due to the heterogeneous physicochemical surface features of the sponge, the conventional techniques, such as sessile drop analysis is not suitable for this application. Alternatively, IGC has the capability to characterize heterogeneous samples.[34] Based on Lewis acid and base theory, γ_{S-V} was calculated as,

$$\gamma_{S-V} = \gamma_{LW} + \gamma_{AB} \tag{2}$$

The Dorris-Gray method was used to measure γ_{S-V} using n-alkanes as the probe molecules,[40] while the γ_{AB} was obtained using Good-van Oss-Chaudhury (GvOC) method, as given by (3)[41]:

$$\gamma_{AB} = (\gamma_S^+ \gamma_S^-)^{\frac{1}{2}} + (\gamma_S^+ \gamma_L^-)^{\frac{1}{2}} \tag{3}$$

where, γ_S^+ and γ_S^- are acid and base surface energies determined using mono-polar solvents, dichloromethane and ethyl acetate for the solid and the liquid.

The γ_{S-V}, γ_{LW}, and γ_{AB} of the SEnS measured at various surface coverages (fractional monolayer coverage) are shown in **Figure 4a**. As can be seen, the surface energy slightly changes with coverage, and it contains different levels of energy sites. Both γ_{LW} (ranges between 17 to 19 mJ m^{-2}) and γ_{AB} (ranges between 47 to 52 mJ m^{-2}) decrease with the increasing surface coverage. The highest energy occurs close to zero surface coverage because the highest adsorption energy sites are easily populated by the incoming probe molecules. Also, the surface energies are almost constant at higher surface coverage. γ_{S-V}, of the SEnS is in the range of 64 to 71 mJ m^{-2}.

Prediction of droplets adhesion based on surface energetics. According to the Baier curve, the low surface tension organic liquids bind in different ways depending on the total surface energy (γ_{S-V}). At low surface energy γ_{AB} values between 10 to 20 mJ m^{-2}, the wetting between the two materials is weak to moderate. At higher values between 40 to 75 mJ m^{-2}, the wetting between two materials is strong.[24,26] As shown in **Figure 4a**, for this material, the major component of total surface energy (γ_{S-V}) comes from dispersion interactions (γ_{LW}), which falls under the region of strong adsorbate adhesion. The high dispersion surface energy is due to the omnipresent physical Lifshitz-van der Waals forces. The higher contribution as well as omnipresence of Lifshitz-van der Waals forces enables effective adsorption of crude oil droplets onto SEnS across all pH conditions.[42,43]

Meanwhile, the minor component of total surface energy comes from the acid-base component (γ_{AB}) which falls under weak to moderate adsorbate adhesion. This pH-dependant γ_{AB} can also be exploited for favorable oil droplet adhesion. This acid-base binding occurs by the electrostatic opposite charge interactions and the charge mediated hydrogen bonding.[41,44] These complementary forces will exist when the pH is between the PZC of the sponge and IEP of the crude oil, as shown in **Figure 4b**.
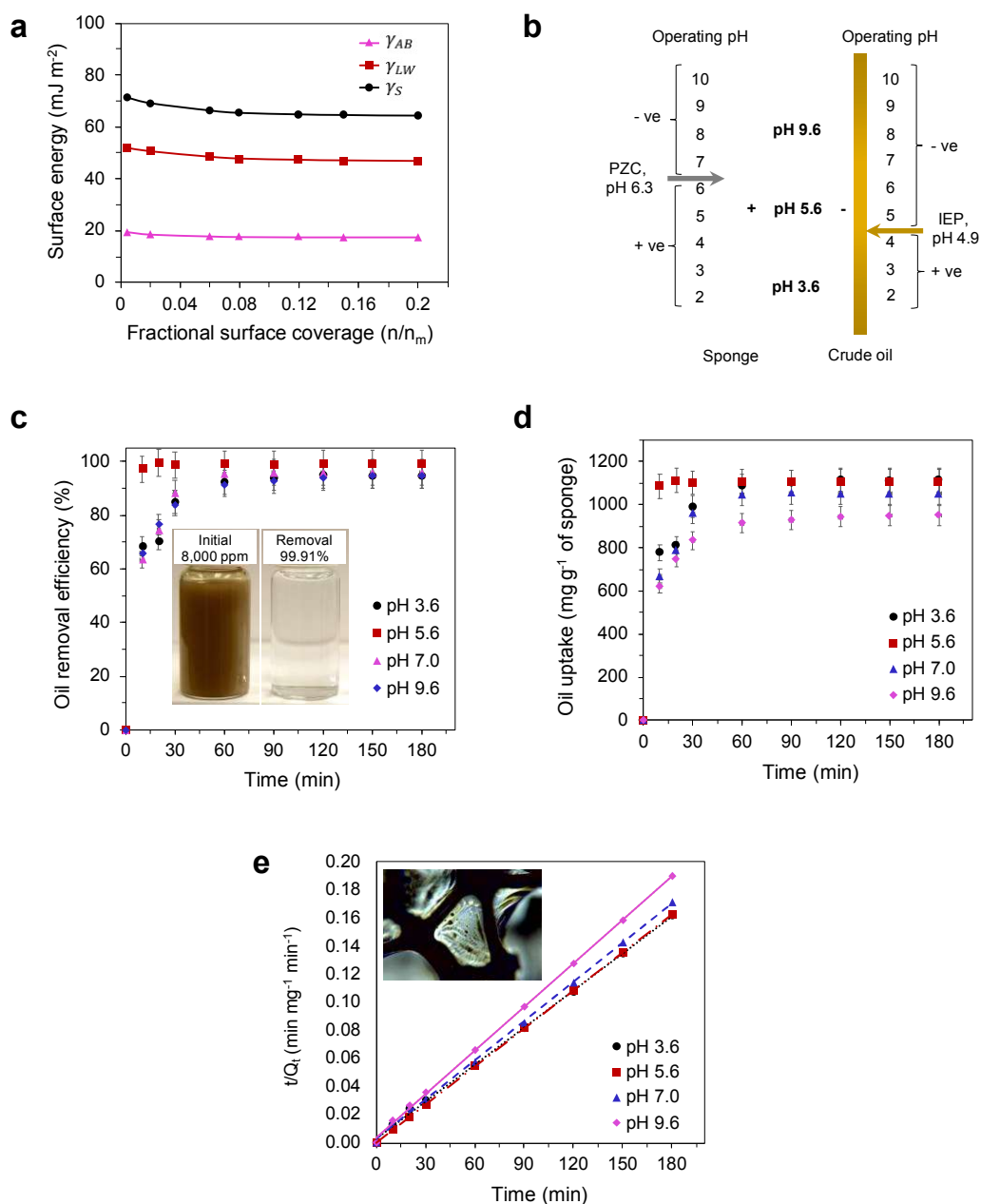
Figure 4. (a) and (b) Hypothesized adsorption mechanisms, (c) and (d) experimental evidence, and (e) theoretical model. (a) SEnS surface energy profile showing total surface energy, dispersive component, and acid-base components. (b) Prediction of best pH range for high probability of crude oil microdroplet adhesion. (c) Influence of pH on oil removal efficiency (at acid, neutral, base, and best pH values). (d) Influence of pH on crude oil uptake. (e) Pseudo-second order kinetic model of the adsorption of crude oil at different pH values. The microscope image (inset) shows the oil droplets deposition on the pore surface.

13

Crude oil adsorption with solution pH and kinetics. The crude oil is a mixture of acid, base, and organic components. The acid and base composition of the oil was measured as 0.6 and 0.9 mg KOH/g. These results indicate that the oil is a stronger base. The isoelectric point (IEP) of the oil microdroplets was previously reported as pH 4.9, indicating that the oil microdroplets were positively charged below pH 4.9 and negatively charged above this pH by ionization of interfacial acid-base groups.

The adsorption experiments were performed using crude oil-in-water emulsions with a droplet size below 10 μm.[9] Based on surface charge characterization, the best adsorption occur at pH 5.6. As such, this pH is compared with a more acidic condition (3.6), neutral (pH 7.0), and more basic condition (pH 9.6). The resulting adsorption of crude oil microdroplets onto SEnS, as shown in **Figure 4c**, was quantified using total organic carbon (TOC) removal. Due to favorable surface energetics, at all pH values, the SEnS is able to adsorb 95-99% of crude oil in less than 180 mins. However, as expected based on the previous surface charge characterization, there was variation in the speed of oil removal according to emulsion pH. The SEnS showed fastest oil removal at best pH of 5.6 (over 92% removal in 10 min). At neutral pH 7, the removal was moderate with 99% removal in 60 min. However, at both extreme acid (pH 3.6) and extreme base (pH 9.6) conditions, the removal was the slowest (~95% removal in 180 min).

The effect of pH on the temporal removal efficiency can be further understood from the zero charge points of the SEnS and crude oil microdroplets.[9] As shown in **Figure 4b**, the zero charge points of the SEnS and crude oil occur at pH 6.3 and 4.9, respectively. Therefore, at pH 5.6, a positive charge exists on the SEnS and a negative charge exists on the oil microdroplet surfaces. Therefore, within this region, fastest adsorption of oil microdroplets onto SEnS is expected due to opposite charge attraction in conjunction with Lifshitz-van der Waals forces. The moderate removal speed at pH 7 is attributed to the Lifshitz-van der Waals forces as the charge on the materials surface is almost zero. On the other hand, at extreme acid and base conditions, the removal is predominantly due to Lifshitz-van der Waals forces as well, however the acid-acid or base-base repulsive interactions might have slowed the adsorption process.

Adsorption kinetics. The experimental kinetics of crude oil uptakes onto the SEnS are shown in **Figure 4d**. The same kinetic model was used to predict the theoretical oil uptake and adsorption mechanisms at all pH values (**Figure 4e**). Here the kinetics are described for the example of neutral pH. The adsorption occurs in two steps, an initial rapid exponential increase (60 min) followed by a slower linear rate (60 to 180 min). The initial rapid adsorption of oil microdroplets is attributed to physisorption onto the larger concentration of adsorption sites on the SEnS surface. The later slow adsorption step is attributed to the lower number of vacant adsorption sites, and hindered pore diffusion by the initially deposited oil film (inset in **Figure 4e**).[45] The kinetic adsorption of the crude oil onto the SEnS was described using a pseudo-second-order kinetic model,[46]

$$\frac{t}{Q_t} = \frac{1}{k_2 Q_e^2} + \frac{t}{Q_e} \tag{4}$$

where Q_e and Q_t represents the amount adsorbed crude oil on the SEnS (mg g^{-1}) at equilibrium and time t (min), and k_2 is the adsorption rate constant (g mg^{-1} min). The t/Q_t versus t plot, shown in **Figure 4e**, demonstrates that the second-order model adequately describes the adsorption phenomenon with an R^2 correlation coefficient in the range of 0.998 to 1.000 for all pH values. The kinetic model described the crude oil adsorption onto the SEnS with a theoretical maximum uptake (Q_t) of 1111 mg g^{-1}, which agrees well with the experimental oil mass uptake (Q_e) of 1047 mg g^{-1} with $k_2 = 2.38 \times 10^{-4}$ g mg^{-1} min. The predicted and experimental values at other pH values are listed in **Table S1**.

Adsorbed oil recovery and SEnS reuse. Compared to traditional adsorbents, the SEnS offers benefits in terms of material reusability and adsorbed crude oil recovery at ambient conditions. The regeneration of the traditional adsorbents requires costly methods, such as high temperature, microwave irradiation or ultrasound due to clogging of the nanometer pores.[47,48] In this current work, due to the very large pore sizes (200 to 1100 μm), the SEnS does not suffer from pore clogging, enabling adsorbed oil recovery at ambient conditions.

The minimum work required to break the binding between the adsorbed oil droplets and the sponge surface, and hence recover the oil, can be determined from work of adhesion. According to Fowkes equation, the thermodynamic work of adhesion between the crude oil microdroplets and the SEnS is estimated as 58 to 66 mJ m^{-2} using:

$$W_{adhesion} = 2(\gamma_{S-V}\gamma_{L-L})^{\frac{1}{2}} \tag{5}$$

where, the crude oil interfacial tension with water (γ_{L-L}), measured using axisymmetric drop shape analysis (ADSA) method, is ~14 mJ m^{-2}.[9] Since the binding between the droplets and the sponge is high, the adsorbed crude oil recovery by the established method of mechanical compression was not effective.[9] Therefore, surface chemical displacement principles[49] were applied to regenerate the SEnS and rapidly recover adhered crude oil film by using a solvent at ambient conditions. This method has the benefits of energy-efficiency and practical implementation. The prerequisites of the cleaning solvent, based on the proposed regeneration mechanism (**Figure 5**), include i) high solubility with crude oil to enable dissolution of the adhered crude oil film (**Figure 5a** and **5b**), ii) lower surface tension than the crude oil to enable the preferential adsorption of the solvent onto the sponge surface (**Figure 5c**), and iii) high vapor pressure to allow ease of residual solvent evaporation from the sponge surface for eventual reuse (**Figure 5d**). Furthermore, the crude oil and solvent can be separated at low temperatures by distillation.

Based on the composition analysis (**Table S2**), the crude oil is enriched with a high concentration of insoluble resins, which readily dissolve in pentane or heptane.[50] In addition to high solubility, pentane offers an appreciably lower surface tension (15 mJ m^{-2}) than the crude oil (24 mJ m^{-2}) and high vapor pressure (53 kPa at 18.5 ℃). Therefore, pentane was selected as the cleansing solvent. The regenerated SEnS was reused to adsorb crude oil microdroplets using a fresh batch of model emulsions for 5 cycles at a pH value of 7.0 with over 99% efficiency (**Figure 5e**). Furthermore,

after 5 adsorption-regeneration cycles, the crude oil and solvent mixture were rapidly separated using a distillation column at 60 °C, above the pentane boiling temperature (**Figure 5f**).
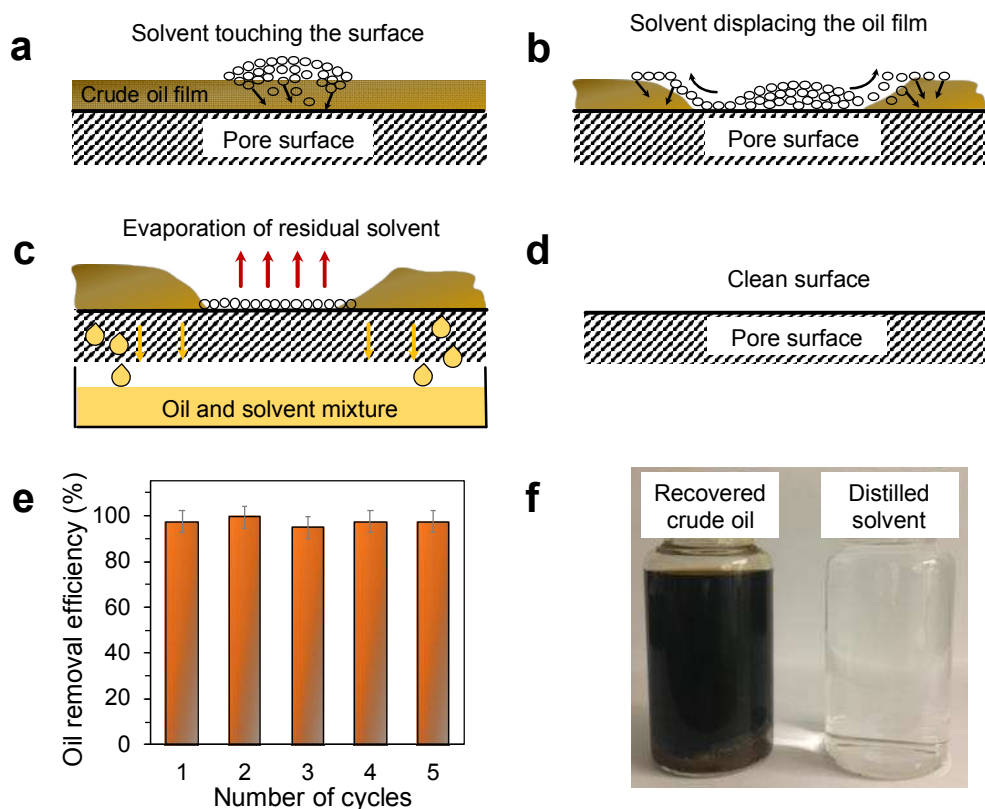

Figure 5. Crude oil recovery and SEnS reuse: (a) to (d) Adsorbed crude oil film displacement mechanism using pentane. (a) Solvent drops contact the oil film. (b) Solvents starting to displace the oil film. (c) Solvent spreading showing the oil displacement and mixture of solvent and oil collection. (d) Subsequently, due to the high vapor pressure, the residual solvent evaporates from the solid surface at ambient conditions. Upon evaporation of the solvent, solid surface will be clean and ready for reuse. (e) Oil removal efficacy versus the number of adsorption cycles for the regenerated sponge at pH 7.0. (f) Adsorbed crude oil and solvent separated using low temperature distillation.

Conclusions

Crude oil is a complex mixture of acid, base, and oleophilic components. In emulsions, the crude oil-water interfacial chemical groups (acid and base) alter the wetting behaviour according to the surrounding water pH. To date, no SEnS was developed to be applicable for a wide range of pH levels to enable effective recovery of crude oil microdroplets.

This work develops a new framework to enable engineering of advanced functional sponges for rapid crude oil microdroplet adsorption. To complement crude oil composition variations, innovative SEnS were designed with heterogeneous chemical groups (acid, based, and organic groups), surface charge, and micro/nano roughness through application of ncSi-decyl nanocoating. The SEnS surface physicochemical properties were characterized using inverse gas chromatography, XPS, and AFM tools. These property changes lowered the sponge surface energy to the range Baier's surface energy levels required for adhesion of low surface tension organic liquids. Based on surface energetics, it was expected that significant oil adsorption would be achieved at all pH values. Furthermore, based on surface charge properties, it was expected that the best pH value for maximum oil adsorption would be at 5.6.

Due to the favorable surface energy, the SEnS could effectively adsorb crude oil microdroplets at all pH values with 95-99% efficiency. The desired surface energy was achieved using nanomaterials at less than 1 wt%, resulting in a low-cost nanocomposite. Furthermore, based on surface charge property of the materials, the predicted best pH for maximum crude oil adsorption was experimentally validated. In addition, to improve economic value, new oil recovery and sponge reuse protocols were developed. Based on surface chemical principles, the strongly adhered crude oil was recovered from SEnS surface by a solvent wash. The cleaned SEnS was reused multiple times for oil adsorption from emulsions. The crude oil was also recovered from the mixture by distillation. In conclusion, this framework develops reusable sponges for effective recovery of crude oil microdroplets from water at broad pH values, enabling new, scalable, nanocomposite-based adsorbents. This work can enable sponge-based water technologies with the potential to revolutionize the remediation of oil field effluents and generate value from the wastewater.

Methods

Materials. Texas raw crude was used for all oil-in-water emulsions. The raw and emulsified properties of the crude oil are described elsewhere.[9] The polyester polyurethane sponge was purchased from a local vendor. The sponge films for AFM were prepared by pressing the sponge in a compression mold at 160 °C. For the sponge surface coating, commercially available ncSi was purchased from Alfa Aesar (crystalline, APS ≈100 nm, 99%, Plasma Synthesized) and 1-decene (98%) was purchased from Sigma-Aldrich. All of the chemicals used in the adsorption experiments were ≥99% concentration and purchased from Sigma Aldrich.

Crude oil characterization. To determine the crude oil saturated, aromatic, resin and asphaltene (SARA) composition, the asphaltenes are isolated by mixing the sample with pentane at a ratio of 1:40. This solution was ultrasonically agitated for at least 30 minutes at room temperature followed by centrifugation and decanting to isolate the asphaltenes. After solvent evaporation of the remaining maltene fraction, an Agilent 1100 Series HPLC is used to separate the maltene fraction into saturated, aromatic, and polar (resin) fractions (SAR) by methods consistent with ASTM D7419, but extended to include the resin fraction. An Evaporative Light Scattering Detector (ELSD) is used to quantify the SAR fractions from the HPLC. SAR fractions are collected for further analysis by an automated sample collector. The SAR compositional data are combined with the asphaltene content (from the precipitation) to calculate the complete SARA composition. The collected fractions are used in any further analyses such as biomarker and isotopic analysis. The SARA analysis plot and fractional distribution are included in the Supporting Information (**Table S2**).

The interfacial tension of the crude oil-water was measured using the axisymmetric drop shape analysis (ADSA) method following the procedure described elsewhere.[51] The change in oil drop shape was monitored for 60 minutes. For adsorption studies, model crude oil-in-water emulsions were prepared using Texas raw crude. The model emulsions were developed with a total organic carbon concentration of ~8,000 mg L^{-1}. The crude oil was mixed with deionized water in a high-speed bender at 22,000 rpm for 30 mins. The characterization of the emulsions was reported elsewhere.[9]

Materials synthesis and coating. The decyl chain was covalently bonded onto the commercial plasma synthesized ncSi by hydrosilylation reaction.[52,53] The Si-H combined with hydrofluoride (HF) etching was reacted with 1-decene to yield decyl-capped ncSi (ncSi:C10).[54-56] For a typical batch synthesis, 0.2 g of ncSi was dispersed in 10 mL of anhydrous ethanol using magnetic stirring and sonication. The solution was mixed with 20 mL of hydrofluoric acid solution (48 wt. % in H_2O) and stirred to remove any surface oxide of the silicon nanocrystals. The ncSi was extracted by washing with 1-decene and the dissolved air was removed using vacuum. The reaction vessel was purged with nitrogen gas and heated up to 170 °C for over 20 hours, to let 1-decene chemically react to the surface of ncSi, yielding surface-modified ncSi. The ncSi:C10 was collected by centrifugation (see transmission electron microscopy or TEM images in **Figure S5** and **BET** plot in **Figure S6**). The TEM images also show the organic corona of the ncSi:C10. In **Figure S7**, the infrared (IR) spectrum of ncSi:C10 confirmed successful surface capping of the ncSi with decyl group, exhibiting the strong CH_x stretching mode at ~2900 cm^{-1}.

The ncSi:C10 was coated onto the sponge by facile dip coating method using hexane dispersion of ncSi:C10 (0.4-0.5 mg mL^{-1}). The redundant dispersion was drained off by gravity and the residual hexane was removed under vacuum. To verify the ncSi:C10 deposition inside the SEnS, the internal sections were visualized under Nikon A1 confocal microscope (**Figure S8**). The images show, the PESPU substrate (green) pore is nicely deposited with ncSi:C10 (brown) on both sides. Experimentally, the lowest amount of ncSi:C10 required for the rapid oil adsorption was determined as < 1 wt.% relative to sponge weight.

Sponge characterization. The BET surface area of the SEnS was characterized using IGC-SEA (Surface Measurement Systems, Alperton, U.K.) The octane vapor and the BET method was applied to calculate the surface area. The octane was selected for the measurement since the large molecule size of octane prevents its diffusion into the polyurethane matrix, which will produce a reliable surface area. The surface microstructures on the sponge surface were observed by optical profiler (Bruker Contour K), FESEM (FESEM, JEOL JSM6610-LV SEM), and AFM (Bruker Bioscope Catalyst).[57,58] The acidity and basicity of the sponge were determined as Gutmann acid and base numbers using IGC.

The fluid wettability inside the porous media was imaged using X-ray micro-CT (ZEISS Xradia VersaXRM-500 X-ray micro-CT) scanner. High resolution 3D images showed the fluid inside the

sponge. Prior to measurements, the sponge samples were cleaned with flowing air. Either crude oil or water was injected into clean and dry samples of size 2x2x2 mm^3 to displace air. The fluids were allowed to reach equilibrium before acquiring 2 μm/voxel scans to characterize *in situ* wettability. The contact angles at the sponge surface in air with water, crude oil, 0.1 M NaOH, and 0.1 M HCl were measured according to the sessile drop method. XPS (ThermoFisher Scientific, E. Grinstead, U.K.) measurements were performed with monochromatic Al Kα X-ray radiation and hemispherical electron energy analysis. The spectra were corrected as per C 1s line at 285 eV and Avantage v.5.926 software was used for curve fitting. The surface charge property of the sponge was measured using SurPASS3 Electrokinetic Analyzer (Anton Paar GmbH, Graz).

Oil adsorption experiments. These adsorption experiments were conducted in batch using model crude oil-water emulsions at different pH values. **Table S2** shows the properties of bulk fluids and emulsions used for the adsorption experiments. The desired pH of the emulsions was adjusted with 0.05 M HCl and 0.05 M NaOH. SEnS samples of ~0.8 g were immersed into 100 mL emulsion, at an initial oil concentration of ~8,000 mg L^{-1} and a range of pH values (3.6, 5.6, 7.0 and 9.6). The experiments were conducted with the emulsion at 40 ℃ and stirred at 500 rpm for a period of 3 h. To determine the oil adsorption efficiency, at predetermined intervals, solution samples were drawn and analyzed using a total organic carbon analyzer (Shimadzu, TOC-VCPN). The adsorption capacity of the sponge was evaluated using,

$$q_e = \frac{(C_0 - C_e)V}{m} \tag{6}$$

where C_0 and C_e represent the initial and instantaneous oil concentrations (mg L^{-1}), V is the volume of the emulsion (L), and m is the mass of the adsorbent (g). The oil removal efficiency was evaluated using,

$$\eta\% = \frac{(C_0 - C_e)}{C_0} X \ 100 \tag{7}$$

For the regeneration and material reuse experiments, the used SEnS was washed using pentane to regenerate after each cycle. The cleaned sponge was reused for adsorption experiments with fresh batch of oil-water emulsion following the protocol described above. To recover the crude oil from

the oil and solvent mixture, the mixture was heated to 60 °C, above the boiling point of the pentane in a distillation setup.

Acknowledgements

Authors information

Affiliations

Department of Mechanical and Industrial Engineering, University of Toronto, Toronto, Canada.
Pavani Cherukupally, Wei Sun, Amy M. Bilton, and Chul B. Park

Department of Chemistry, University of Toronto, Toronto, Canada.
Wei Sun, Anabelle P.Y. Wong, Geoffrey A. Ozin

Centre for Microfluidics in Chemistry and Biology, University of Toronto, Toronto, Canada.
Lindsey Fiddes

Department of Chemical Engineering, Imperial College London, London, United Kingdom.
Pavani Cherukupally, Daryl R. Williams

Contributions

P.C. conceived material design, adsorption-regeneration method, planned the study, performed experiments, analysed data, wrote the manuscript, and co-ordinated the project. W.S. conceived nanomaterials synthesis, performed experiments, wrote methodology and performed distillation. L.F. performed AFM, confocal, and optical profilometry measurements. A.P.Y.W. assisted W.S. in materials fabrication. D.R.W. contributed to the sponge characterization, regeneration methodology and sponsored the surface energy studies. G.A.O. proposed ncSi application for water treatment, advised and sponsored materials synthesis, fabrication and commented on the manuscript. A.M.B. defined metrics for practicality, advised the entire project, outlined and edited the manuscript. C.B.P. proposed sponge application for emulsions separation, advised entire project, edited the manuscript, and sponsored the research. A.M.B. is the co-investigator and C.B.P. is the principle investigator of the project. All the authors reviewed and commented on the manuscript.

Competing interest

The authors declare no competing financial interest.

Corresponding author

Correspondence to Chul B. Park (park@mie.utoronto.ca), Amy M. Bilton (bilton@mie.utoronto.ca), and Geoffrey A. Ozin (gozin@chem.utoronto.ca).

References

1. Clark, C. E., & Veil, J. A. Produced water volumes and management practices in the United States. Argonne National Laboratory (ANL), Project No. ANL/EVS/R-09-1 (2009). Weblink accessed on 20 March 2018.

2. Schindler, D. Tar sands need solid science. *Nature* **468**, 499-501 (2010).

3. Kurek, J., Kirk, J.L. Muir, D.C., Wang, X., Evans, M.S., & Smol, J.P. Legacy of a half century of Athabasca oil sands development recorded by lake ecosystems. *PNAS* **110**, 1761-1766 (2013).

4. Ali I. & Gupta V.K. Advances in water treatment by adsorption technology. *Nat. Protoc.* **1**, 2661-2667 (2007).

5. Wang, C., Liu, X., Demir, N.K., Chen, J.P., & Li, K. Applications of water stable metal organic frameworks. *Chem. Soc. Reviews* **45**, 5107-5134 (2016).

6. Li, R., Lianbin, Z., & Peng, W. Rational design of nanomaterials for water treatment *Nanoscale* **7**, 17167-17194 (2015).

7. Xu, L., Yuning C., Na, L., Weifeng Z., Yang Y., Yingze C., Xin L., Yen W., & Lin F. Breathing demulsification: A three-dimensional free-standing superhydrophilic sponge. *ACS Appl. Mater. Interfaces* **7**, 22264-22271 (2015).

8. Li, J., Xu, C., Zhang, Y., Wang, R., Zha, F. & She, H. Robust superhydrophobic attapulgite coated polyurethane sponge for efficient immiscible oil/water mixture and emulsion separation. *J. Mater. Chem. A* **4**, 15546-15553 (2016).

9. Cherukupally P., Acosta E.J., Hinestroza J.P., Bilton A.M., & Park C.B. Acid-base polymeric foams for the adsorption of micro-oil droplets from industrial effluents. *Environ. Sci. Technol.* **51**, 8552-8560 (2017).

10. Rizvi A., Chu R.K. M., Lee J. H., & Park C. B. Superhydrophobic and oleophilic open-cell foams from fibrillar blends of polypropylene and polytetrafluoroethylene. *ACS Appl. Mater. Interfaces* **6**, 21131-21140 (2014).

11. Kiran S.K., Acosta E.J. & Moran K. Study of solvent-bitumen-water rag layers. *Energy Fuels* **23**, 3139-3149 (2009).

12. Kiran S.K., Ng S. & Acosta E.J. Impact of asphaltenes and naphthenic amphiphiles on the phase behavior of solvent-bitumen-water systems. *Energy Fuels* **25**, 2223-2231 (2011).

13. Buckley, J.S., Takamura, K. & Morrow, N.R. Influence of electrical surface charges on the wetting properties of crude oils. *SPE Res. Eng.* **4**, 332-340 (1989).

14. Buckley, J.S., Liu, Y. & Monsterleet, S. Mechanisms of wetting alteration by crude oils. *SPE Journal* **3**, 54-61 (1998).

15. Zisman, W. A. Influence of constitution on adhesion. *Ind. Eng. Chem.* **55**,18-38 (1963).

16. Chaudhury, M.K. & Whitesides, G.M. Correlation between surface energy and surface constitution. *Science* **255**, 1230-1232, (1992).

17. McCarty, L.S. & Whitesides, G.M. Electrostatic charging due to separation of ions at interfaces: Contact electrification of ionic electrets. *Angew. Chemi., Int. Ed.* **47**, 2188-2207 (2008).

18. Lee, A.S., Bütün, V., Vamvakaki, M., Armes, S.P., Pople, J.A., & Gast, A.P. Structure of pH-dependent block copolymer micelle: Charge and ionic strength dependence. *Macromolecules* **35**, 8540-8551 (2002).

19. Yu, X., Wang, Z., Jiang, Y., Shi, F., & Zhang, X. Reversible pH-responsive surface: From superhydrophobicity to superhydrophilicity. *Adv. Mater.* **17**, 1289-1293 (2005).

20. Isa, L., Lucas, F., Wepf, R., & Reimhult, E. Measuring single-nanoparticle wetting properties by freeze-fracture shadow-casting cryo-scanning electron microscopy. *Nature Commun.* **2**, 438, 1-9 (2011).

21. Qu, L.T., Dai, L.M., Stone, M., Xia, Z.H. & Wang, Z.L. Carbon nanotube arrays with strong shear binding-on and easy normal lifting-off. *Science* **322**, 238-242 (2008).

22. Zhang, D., Cheng, Z., Kang, H., Yu, J., Liu, Y.M. & Jiang, L. Smart superwetting surface with responsivity in both surface chemistry and microstructure. *Angew. Chem. Int. Ed.* DOI 10.1002/anie.201800416 (2018).

23. Baier R.E., Shafrin E.G. & Zisman W.A. Adhesion: Mechanisms that assist or impede it. *Science* **162**, 1360-1368 (1968).

24. Baier, R.E. The role of surface energy in thrombogenesis. *Bull. N. Y. Acad. Med.* **48**, 257-272 (1972).

25. Absolom, D.R., Lamberti, F.V., Policova, Z., Zingg, W., Van Oss, C.J., & Neumann, A. W. Surface thermodynamics of bacterial adhesion. *Appl. Environ. Microbiol.* **46**, 90-97 (1983).

26. Baier, R.E., Michlovic, J.G., Depalma, V.A., & Pilie, R.J. Universal gelling agent for the control of hazardous liquid spills. *J. Hazard. Mater.* **1**, 21-33 (1975).

27. Tie, L., Zhiguang, G., & Weimin, L. pH-manipulated underwater-oil adhesion wettability behavior on the micro/nanoscale semicircular structure and related thermodynamic analysis. *ACS Appl. Mater. Interfaces* **7**, 10641-10649 (2015).

28. Croissant, J.G., Fatieiev, Y., & Khashab, N.M. Degradability and clearance of silicon, organosilica, silsesquioxane, silica mixed oxide, and mesoporous silica nanoparticles. *Adv. Mater.* **29**, 1604634 (2017).

29. Zhou, Y., Ellis, M.W., Nain, A.S. & Behkam, B. Effect of electrode sub-micron surface feature size on current generation of Shewanella oneidensis in microbial fuel cells. *J.Power Sources* **347**, 270-276 (2017).

30. Briggs, D., Brewis, D.M., Dahm, R.H., & Fletcher, I.W. Analysis of the surface chemistry of oxidized polyethylene: Comparison of XPS and ToF-SIMS. *Surf. Interface Anal.* 35, 156-167 (2003).

31. Andoa, R.A., do Nascimento, G.M., Landers, R., & Santos, P.S. Spectroscopic investigation of conjugated polymers derived from nitroanilines. *Spectrochim. Acta A* 69, 319 (2008).

32. Yu, Y., Hessel, C. M., Bogart, T. D., Panthani, M. G., Rasch, M. R., & Korgel, B. A. Room temperature hydrosilylation of silicon nanocrystals with bifunctional terminal alkenes. *Langmuir* 29, 1533-1540 (2013).

33. Saint Flour, C., & Papirer, E. Gas-solid chromatography: A quick method of estimating surface free energy variations induced by the treatment of short glass fibers. *J. Colloid. Interface Sci.* **91**, 69-75 (1983).

34. Burnett, D.J., Khoo, J., Naderi, M., Heng, J.Y.Y., Wang, G.D., & Thielmann, F. Effect of processing route on the surface properties of amorphous indomethacin measured by inverse gas chromatography. *AAPS Pharm. Sci. Tech.* **13**, 1511-1517 (2012).

35. Fowkes, F.M. Quantitative characterization of the acid-base properties of solvents, polymers, and inorganic surfaces. *J. Adhes. Sci. Technol.* **4**, 669-691 (1990).

36. Salamone, J.C. Polymeric materials encyclopedia; CRC: Boca Raton, FL, 1895-1895 (1998).

37. Dukhin, S.S., & Derjaguin, B.V. Non-equilibrium double layer and electrokinetic phenomena. In Surface and Colloid Science, Matijevic, E., Ed., J. Wiley & Sons: New York, **7**, 297-300 (1974).

38. Hunter, R.J. Electrified interfaces: The Electrical Double Layer Foundations of Colloid Science, Oxford University Press Inc: New York, **2**, 317-325 (2001).

39. Zimmermann, R., Freudenberg, U., Schweiß, R., Küttner, D., & Werner, C. Hydroxide and hydronium ion adsorption. *Curr. Opin. Colloid Interface Sci.* **15**, 196-202 (2010).

40. Dorris, G.M., & Gray, D.G. Adsorption of n-alkanes at zero surface coverage on cellulose paper and wood fibers. *J. Colloid Interface Sci.* **77**, 353-362 (1980).

41. Van Oss, C.J., Good, R.J., & Chaudhury, M.K. Additive and nonadditve surface tension components and the interpretation of contact angles. *Langmuir* **4**, 884-891 (1988).

42. Van Oss, C.J. Interfacial forces in aqueous media. Marcel Dekker: New York, NY, 1994.

43. Ambrosetti, A., Ferri, N., DiStasio, R.A., & Tkatchenko, A. Wavelike charge density fluctuations and van der waals interactions at the nanoscale. *Science* **351**, 1171-1176 (2016).

44. Valtiner, M., Donaldson Jr, S.H., Gebbie, M.A. & Israelachvili, J.N. Hydrophobic forces, electrostatic steering, and acid-base bridging between atomically smooth self-assembled monolayer and end-functionalized PEGolated lipid layers. *J. Am. Chem. Soc.* **134**, 1746-1753, (2012).

45. Swain, S.K., Mishra, S., Sharma, P., Patnaik, T., Singh, V.K., Jha, U., Patel, R.K. & Dey, R. K. Development of a new inorganic-organic hybrid ion-exchanger of zirconium (iv)-propanolamine for efficient removal of fluoride from drinking water. *Ind. Eng. Chem. Res.* **49**, 9846-9856 (2010).

46. Ho, Y.S. & McKay, G. Pseudo-second order model for sorption processes. *Process Biochem.* **34**, 451-465 (1999).

47. Guilane, S. & Hamdaoui, O. Regeneration of exhausted granular activated carbon by low frequency ultrasound in batch reactor. *Desalin. Water Treat.* **57**, 15826-15834 (2016).

48. Qu, W., Hu, Q., Zhu, Y., Peng, J. & Zhang, L. Microwave-assisted regeneration of spent activated carbon containing zinc acetate and its application for removal of congo red. *Desalin. Water Treat.* **57**, 28496-28511 (2016).

49. Baier, R.E., Meyer, A.E., & Akers, C.K. Safe and effective decontamination of delicate surfaces. *Bioeng II* 293-296 (1983).

50. Demirbas, A., & Taylan, O. Removing of resins from crude oils. *Petrol. Sci. Technol.* **34**, 771-777 (2016).

51. Kwok, D.Y., Vollhardt, D., Miller, R., Li, D., & Neumann, A.W. Axisymmetric drop shape analysis as a film balance. *Colloids Surf. A* **88**, 51-58 (1994).

52. Sun, W., Qian, C., Mastronardi, M.L., Wei, M., & Ozin, G. A. Hydrosilylation kinetics of silicon nanocrystals. *Chem. Comm.* **49**, 11361-11363 (2013).

53. Sun, W. et.al., Switching-on quantum size effects in silicon nanocrystals. *Adv. Mater.* **27**, 746-749 (2015).

54. Mangolini, L., Jurbergs, D., Rogojina, E., & Kortshagen, U. Plasma synthesis and liquid-phase surface passivation of brightly luminescent Si nanocrystals. *J. Lumin.* **121**, 327-334 (2006).

55. Pi, X.D., Mangolini, L., Campbell, S.A., & Kortshagen, U. Room-temperature atmospheric oxidation of Si nanocrystals after HF etching. *Phys. Rev. B* **75**, 085423 (2007).

56. Sun, W. et.al., Silicon monoxide–a convenient precursor for large scale synthesis of near infrared emitting monodisperse silicon nanocrystals. *Nanoscale* **8**, 3678-3684 (2016).

57. Rizvi, A., Tabatabaei, A., Vahedi, P., Mahmood, S. H., & Park, C. B. Non-crosslinked thermoplastic reticulated polymer foams from crystallization-induced structural heterogeneities. *Polymer* **135**, 185-192 (2018).

58. Hamidinejad, S. M., Chu, R. K., Zhao, B., Park, C. B., & Filleter, T. Enhanced thermal conductivity of graphene nanoplatelet-polymer nanocomposites fabricated via supercritical fluid assisted in-situ exfoliation. *ACS Appl. Mater. Interfaces* **10**, 1225-1236 (2018).

Adsorptive Recovery of Emulsified Crude Oil from Water Using Surface Engineered Sponge

Pavani Cherukupally, Wei Sun, Anabelle P.Y. Wong, Daryl R. Williams, Geoffrey A. Ozin, [*]

Amy M. Bilton, [*] and Chul B. Park[*]
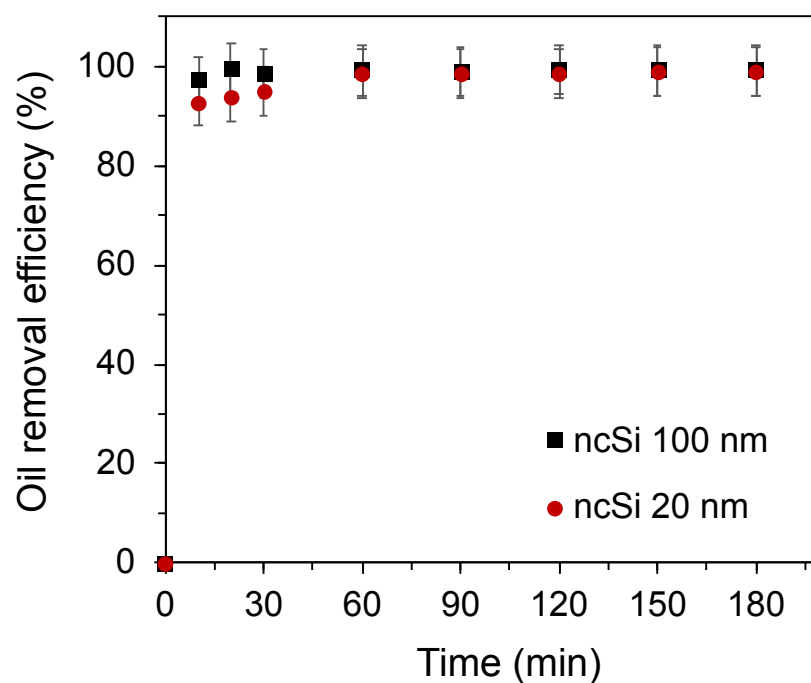
Supporting Figures

Figure S1. Variation in crude oil removal efficiency due to nanomaterial particle size. The SEnS coated with 100 nm exhibited a higher rate of removal than the 20 nm at less than 1 wt% of ncSi.
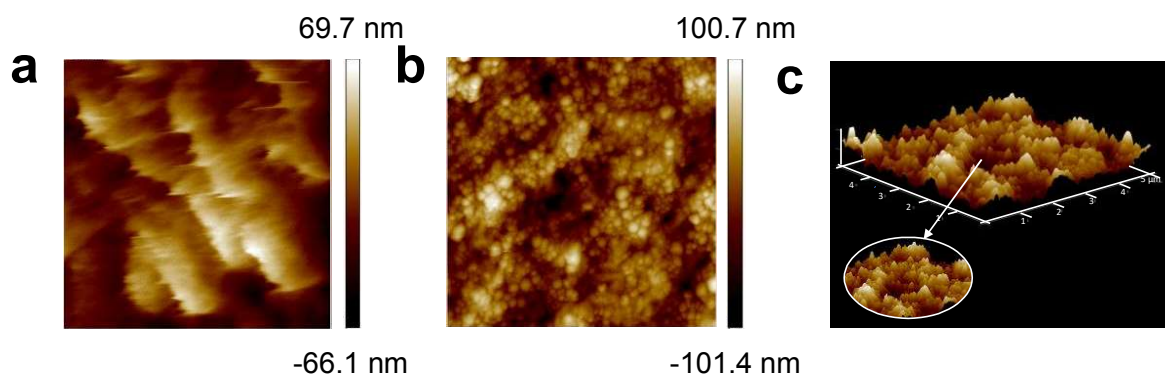
Figure S2. AFM micrographs at different resolutions: (a) nano wrinkles at the surface (1x1 μm). (b) ncSi spherical shape (5x5 μm). (c) long-range structures represent the typical shape of hydrophobicity.[1]
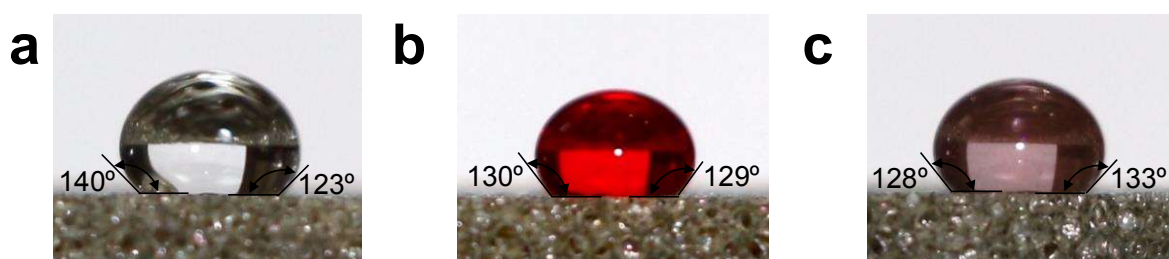
Figure S3. SEnS contact angle with (a) water, (b) 0.1 M HCl, and (c) 0.1 M NaOH showing good hydrophobicity and stability against acid and base liquids.
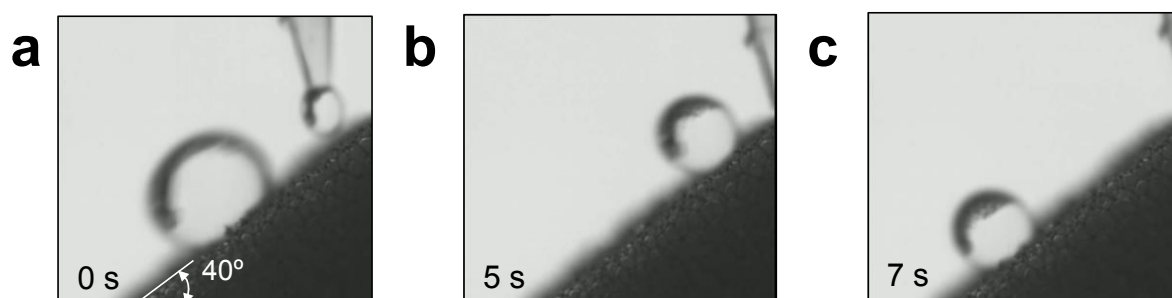

Figure S4. Self-cleaning property of the SEnS. The water droplets effectively rolled off the SEnS surface at an inclination of approximately 40 degrees.
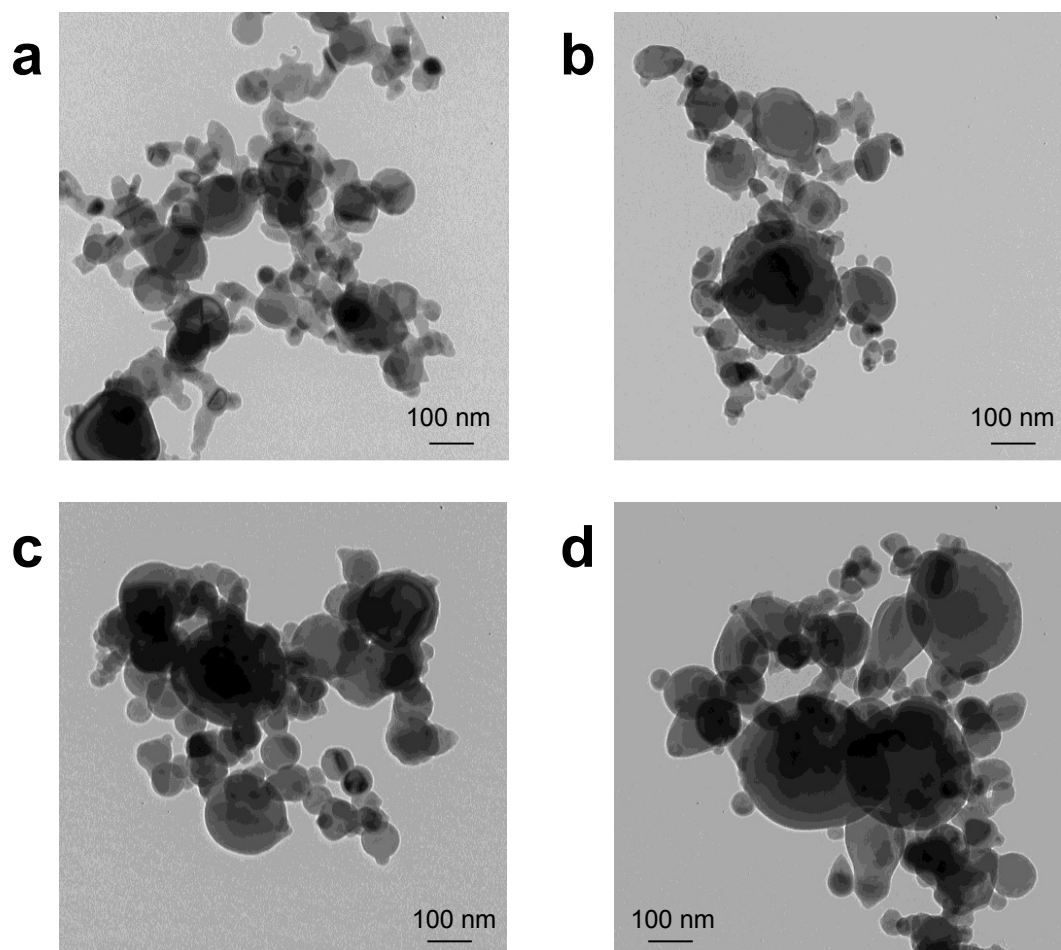
Figure S5. TEM images of nanocrystalline silicon capped with decyl groups. The particles have variable sizes, with an average around 100 nm. Despite the appearance, the ncSi particles are not agglomerated, they are simply stacked together. The grouped size of the particles was between 500 and 600 nm. A thin organic corona on the silicon particles can be observed, in good agreement with the IR spectrum showing the hydrocarbon capping.
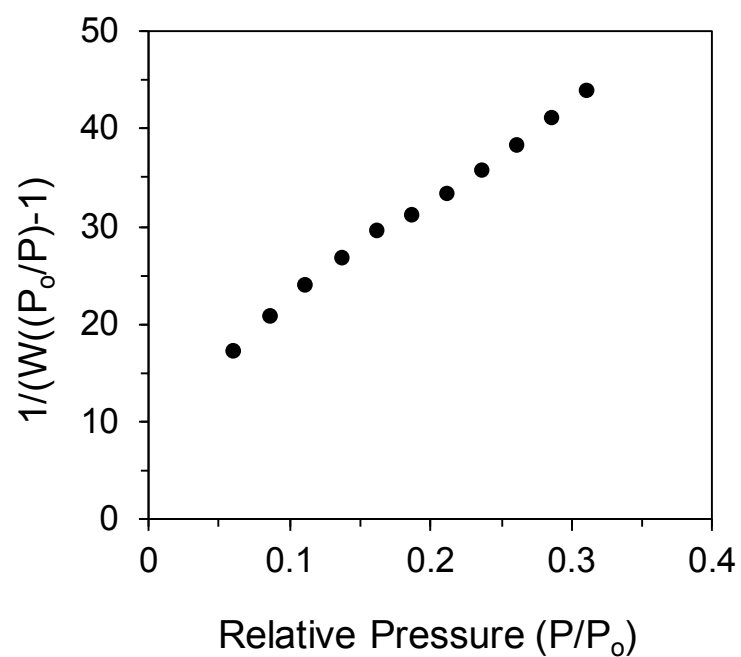
Figure S6. BET plot, generated using N_2 gas, used to determine the surface area of the ncSi. The measurements show that the ncSi possessed surface area of 30.7 m^2/g.
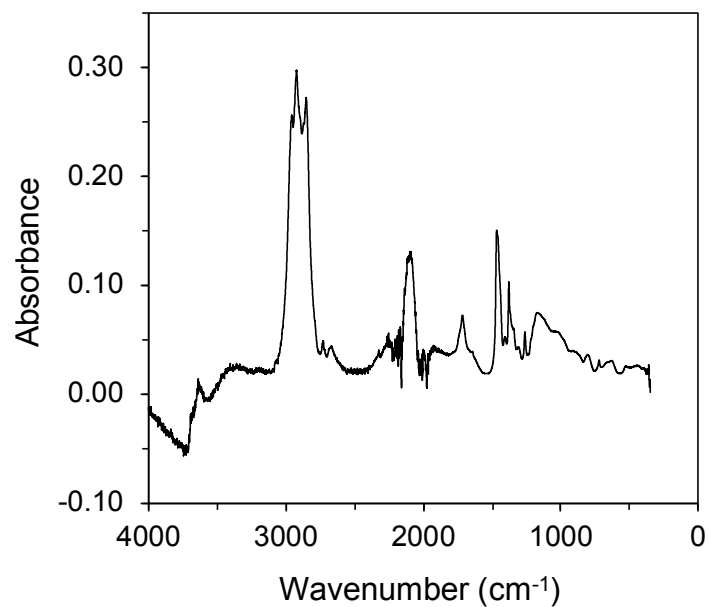

Figure S7. IR spectra of the ncSi:C10 showing decyl is effectively capped on the ncSi.
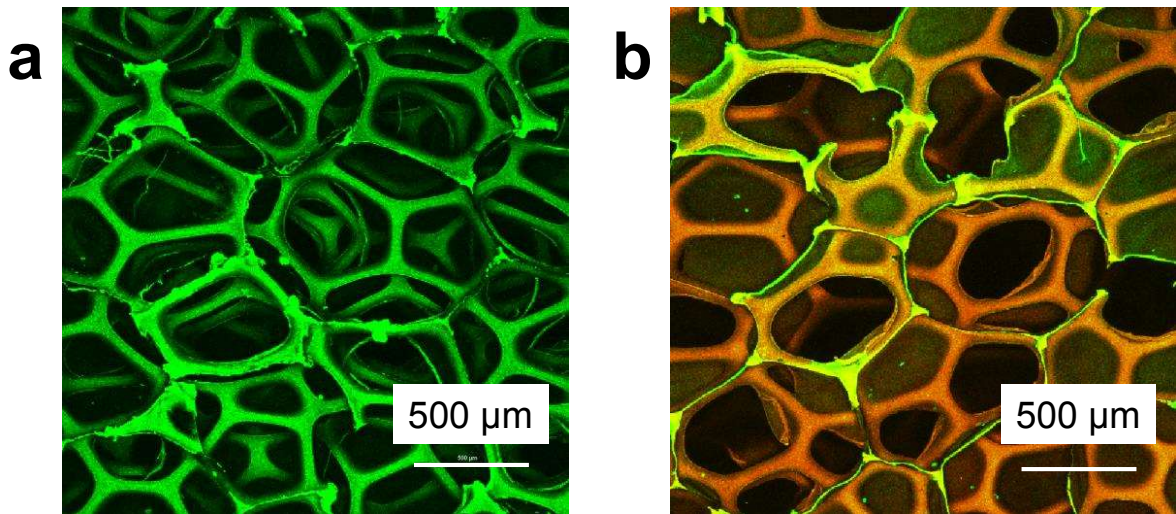
Figure S8. Confocal images of the sponge (a) before nanocoating (b) after nanocoating.

Supporting Tables

Table S1. Predicted theoretical oil uptake and rate constant

Condition (pH)	Theoretical uptake, Q_t (mg/g)	Rate constant, k_2 (g mg^{-1} min)	R^2 value	Experimental uptake, Q_e (mg/g)
3.6	1111	2.38E-04	0.998	1113
5.6	1111	1.16E-02	0.999	1107
7.0	1111	2.38E-04	0.998	1052
9.6	1000	2.44E-04	0.999	950

Table S2. Crude oil and emulsion properties

Property	Value
Composition	
Saturates	62.95%
Aromatics	37.05%
Resins	8.7%
Asphaltenes	1.19%
Base number	0.9 mg KOH/g
Acid number	0.6 mg KOH/g
Droplet size[2]	<10 μm
Polydispersity Index (PDI)	~0.5
Isoelectric point (IEP)[2]	pH 4.9
Interfacial tension at 40 °C	~14.75 mJ m^{-2}

References

1. Isa, L., Lucas, F., Wepf, R., & Reimhult, E. Measuring single-nanoparticle wetting properties by freeze-fracture shadow-casting cryo-scanning electron microscopy. *Nature Commun.* **2**, 438, 1-9 (2011).

2. Cherukupally P., Acosta E.J., Hinestroza J.P., Bilton A.M., & Park C.B. Acid-base polymeric foams for the adsorption of micro-oil droplets from industrial effluents. *Environ. Sci. Technol.* **51**, 8552-8560 (2017).